JOURNAL OF APPLIED CRYSTALLOGRAPHY

Volume 56 (2023)

Supporting information for article:

Anisotropy factors in small-angle scattering for dilute rigid-rod suspensions

Jack Rooks, Peter H. Gilbert, Lionel Porcar, Yun Liu and Paul Butler

S1. Geometric definition of α

This section details the geometric foundations for equation (5):

$$\cos\alpha = -\sin\theta_{\mathrm{p}}\cos\theta_{\mathrm{s}}\cos\left(\phi_{\mathrm{p}} - \phi_{\mathrm{s}}\right) + \cos\theta_{\mathrm{p}}\sin\theta_{\mathrm{s}} \tag{S1}$$

where the orientation angles $(\theta_{\mathrm{p}}, \phi_{\mathrm{p}})$ and the scattering angles $(2\theta_{\mathrm{s}}, \phi_{\mathrm{s}})$ define the angle α between the particle axis, $\vec{L}$, and the scattering vector, $\vec{q}$. We begin with the definition of $\vec{q}$:

$$\vec{q} = \vec{k}_{\mathrm{i}} - \vec{k}_{\mathrm{s}} \tag{S2}$$

where $\vec{k}_{\mathrm{i}}$ is the incident beam wavevector and $\vec{k}_{\mathrm{s}}$ is the scattered neutron wavevector. Each of the vectors can be expressed in Cartesian coordinates, where the particle length is:

$$\vec{L} = \left(L\sin\theta_{\mathrm{p}}\cos\phi_{\mathrm{p}}\,, L\cos\theta_{\mathrm{p}}\,, L\sin\theta_{\mathrm{p}}\sin\phi_{\mathrm{p}}\right) \tag{S3}$$

the incident wavevector is:

$$\vec{k}_{\mathrm{i}} = (0, k, 0) \tag{S4}$$

the elastically scattered wavevector is:

$$\vec{k}_{\mathrm{s}} = (k\sin 2\theta_{\mathrm{s}}\cos\phi_{\mathrm{s}}\,, k\cos 2\theta_{\mathrm{s}}\,, k\sin 2\theta_{\mathrm{s}}\sin\phi_{\mathrm{s}}) \tag{S5}$$

the scattering vector is:

$$\vec{q} = (-k\sin 2\theta_{\mathrm{s}}\cos\phi_{\mathrm{s}}\,, k(1-\cos 2\theta_{\mathrm{s}}), -k\sin 2\theta_{\mathrm{s}}\sin\phi_{\mathrm{s}}) \tag{S6}$$

and k is the magnitude of the incident and scattering wavevectors for elastic scattering.

α is the angle between the primary particle axis and the scattering vector defined by:

$$\cos\alpha \equiv \frac{\vec{L}\cdot\vec{q}}{|\vec{L}||\vec{q}|} \tag{S7}$$

where:

$$\left|\vec{L}\right| = L \tag{S8}$$

and:

$$|\vec{q}| = q = 2k \sin\theta_s \tag{S9}$$

Substituting Eqs. (S3), (S6), (S8) and (S9) into equation (S7) yields:

$$\cos\alpha = \frac{L \sin\theta_p \cos\phi_p \left(-k \sin 2\theta_s \cos\phi_s\right) + L \cos\theta_p \left(k(1-\cos 2\theta_s)\right) + L \sin\theta_p \sin\phi_p \left(-k \sin 2\theta_s \sin\phi_s\right)}{2kL \sin 2\theta_s} \tag{S10}$$

which simplifies to:

$$\cos\alpha = -\sin\theta_p \cos\theta_s \cos\left(\phi_p - \phi_s\right) + \cos\theta_p \sin\theta_s \tag{S11}$$

For backscattering $(2\theta_s = \pi, \phi_s = 0)$ from a particle perpendicular to the vorticity direction ($\phi_p = 0$), α approaches 0 and $\frac{\pi}{2}$ at $\theta_p = 0$ and $\frac{\pi}{2}$, as expected. equation (S11) matches equation (4.40) of (Fuller, 1995) except for a change in sign resulting from an alternative definition for $\vec{q} = \vec{k}_s - \vec{k}_i$, which differs from equation (S2) by a negative sign.

S2. Bin count, annular area and alignment factor

Fig. S2 summarizes the bin counts and annular areas used to calculate alignment factor in **Fig. 7** for a 2D theoretical scattering pattern of cylindrical particles having $L = 1800$ Å, $R = 20$ Å, and 5 % radial polydispersity. The minimum bin count was allowed to drop below the recommended 20 bins to give an idea of the alignment factor at low-q, where 20 bins could not be achieved for the finite detector grid spacing used. The reported annular area is the smallest that can be achieved while maintaining the minimum bin count for a square detector grid spacing of $d = 0.001$ Å^{-1}. This minimum annular area can be generalized to other square detector grid spacings using:

$$A_{A,2} = \left(\frac{d_2}{d_1}\right)^2 A_{A,1} \tag{S1}$$

where d_1 is the distance between adjacent data points for **Fig. 2** and **Fig. 7** of 0.001 Å^{-1}, d_2 is the distance between data points for a second detector grid spacing, $A_{A,1}$ is the annular area using d_1 and $A_{A,2}$ is the estimated annular area for d_2. equation (S1) can be

used as a starting point for finding the inner and outer radii which satisfy the bin requirement for any grid spacing.

When bin count is held constant and $\bar{q}$ increases up to $\bar{q} \approx 0.007$ Å^{-1}, the annular area decreases, where each sharp increase in **Fig. S2b** and **Fig. S2d** corresponds to an increase in bin count (**Fig. S2a** and **Fig. S2c**). The pattern in annular area disappears at $\bar{q} > 0.007$ Å^{-1} because the bin count is not increased beyond the recommended minimum of 20 bins. This allows annular area to vary depending on how well pixels fit within the annulus at each $\bar{q}$.

Rod tilt relative to the neutron beam, θ_{p}, does not influence the bin selection or the annular area chosen, where points for each θ_{p} in **Fig. S2** lie on top of each other. Bin selection and annular area are independent of the scattering particle and are reliant only upon the data resolution and available q-range.

Table S1: Dimensional variables

$L \equiv$ length; $M \equiv$ mass; $t \equiv$ time; $T \equiv$ temperature; $\mathbb{R} \equiv$ All real numbers

Name	Symbol	Dimensions	Range
Annular area	A_{A}	L^{-2}	$0 \leq A_{\mathrm{A}}$
Average scattering vector	$\bar{q}$	L^{-1}	$0 \leq \bar{q}$
Background scattering	B	L^{-1}	$0 \leq B \leq \infty$
Detector grid spacing, nearest neighbor	d	L^{-1}	$0 < d$
Diameter, cylinder	D	L	$0 \leq D$
Flow velocity vector	$\vec{v}$	Lt^{-1}	$\mathbb{R}$
Form factor	$P(q,\alpha)$	L^{2}	$0 \leq P(q,\alpha)$
Form function	$F(q,\alpha)$	L	$0 \leq F(q,\alpha)$
Length, cylinder	L	L	$0 \leq L$
Length, projected cylinder	L_{c}	L	$0 \leq L_{\mathrm{c}}$
Particle Volume	V_{p}	L^{3}	$0 \leq V_{\mathrm{p}} \leq \infty$
Radius, cylinder	R	L	$0 \leq R$
Relaxation Time	λ_{R}	t	$0 \leq \lambda_{\mathrm{R}}$
Scattering axis, normal to incident beam-vorticity plane	$\vec{q}_{\mathrm{x}}$	L^{-1}	$\mathbb{R}$
Scattering axis, parallel to vorticity axis	$\vec{q}_{\mathrm{y}}$	L^{-1}	$\mathbb{R}$
Scattering intensity	$I(q,\alpha)$	L^{-1}	$0 \leq I(q,\alpha)$
Scattering intensity, parallel to cylinder axis	$I_{\parallel}(q)$	L^{-1}	$0 \leq I_{\parallel}(q)$
Scattering intensity, perpendicular to cylinder axis	$I_{\perp}(q)$	L^{-1}	$0 \leq I_{\perp}(q)$
Scattering Length Density Difference (contrast)	$\Delta\rho$	L^{-2}	$\mathbb{R}$

Scattering Vector Magnitude	q	L^{-1}	$0 \leq q$
Scattering vector range for integration or annular averaging	Δq	L^{-1}	$0 \leq \Delta q$
Total Volume	V	L^3	$0 \leq V \leq \infty$
Viscosity, zero-shear	η_0	$ML^{-1}t^{-1}$	$0 < \eta_0$
Wave vector, incident beam	$\vec{k}_\mathrm{i}$	L^{-1}	$\mathbb{R}$
Wave vector, magnitude	k	L^{-1}	$0 \leq k$
Wave vector, scattered	$\vec{k}_\mathrm{s}$	L^{-1}	$\mathbb{R}$
Wavelength	λ	L	$0 < \lambda$
x-coordinate axis, normal to incident beam-vorticity plane	$\vec{x}$	L	$\mathbb{R}$

Table S2: Dimensionless variables

Name	Symbol	Range
Alignment factor	A_{f}	$-2 \leq A_{\mathrm{f}} \leq 1$
Alignment factor, cosine expansion	$A_{\mathrm{f,cos}}$	$-1 \leq A_{\mathrm{f,cos}} \leq 1$
Alignment factor, integrated axes	$A_{\mathrm{f,int}}$	$-\infty \leq A_{\mathrm{f,int}} \leq 1$
Alignment factor, Legendre expansion	$A_{\mathrm{f,L}}$	$-2 \leq A_{\mathrm{f,L}} \leq 1$
Angle between $\vec{q}$ and $\vec{L}$	α	$0 \leq \alpha < 2\pi$
First Bessel function zero	$j_{1,1}$	$j_{1,1} = 3.8317$
First order Bessel function of the first kind	$\mathrm{J}_1(qR\sin\alpha)$	$-0.4 < \mathrm{J}_1(qR\sin\alpha) < 0.6$
Form factor, normalized	$\tilde{P}(q,\alpha)$	$0 \leq \tilde{P}(q,\alpha) \leq 1$
Half-Angle Between Incident and Scattered Neutrons	θ_{s}	$0 \leq \theta_{\mathrm{s}} \leq \frac{\pi}{2}$
Particle orientation angle, azimuthal	θ_{p}	$0 \leq \theta_{\mathrm{p}} \leq \pi$
Particle orientation angle, azimuthal	ϕ_{p}	$0 \leq \phi_{\mathrm{p}} \leq \pi$
Scattering angle, azimuthal	ϕ_{s}	$0 \leq \phi_{\mathrm{s}} \leq 2\pi$
Scattering angle, primary scattering axis	$\phi_{\mathrm{s,0}}$	$0 \leq \phi_{\mathrm{s,0}} < 2\pi$
Sector angle, azimuthal	ϕ_{sect}	$0° \leq \phi_{\mathrm{sect}} \leq 90°$
Sector width	$\Delta\phi_{\mathrm{sect}}$	$0° \leq \Delta\phi_{\mathrm{sect}} \leq 180°$
Structure Factor	$S(q)$	$0 < S(q) \leq \infty$
Volume fraction	ϕ	$0 \leq \phi \leq 1$

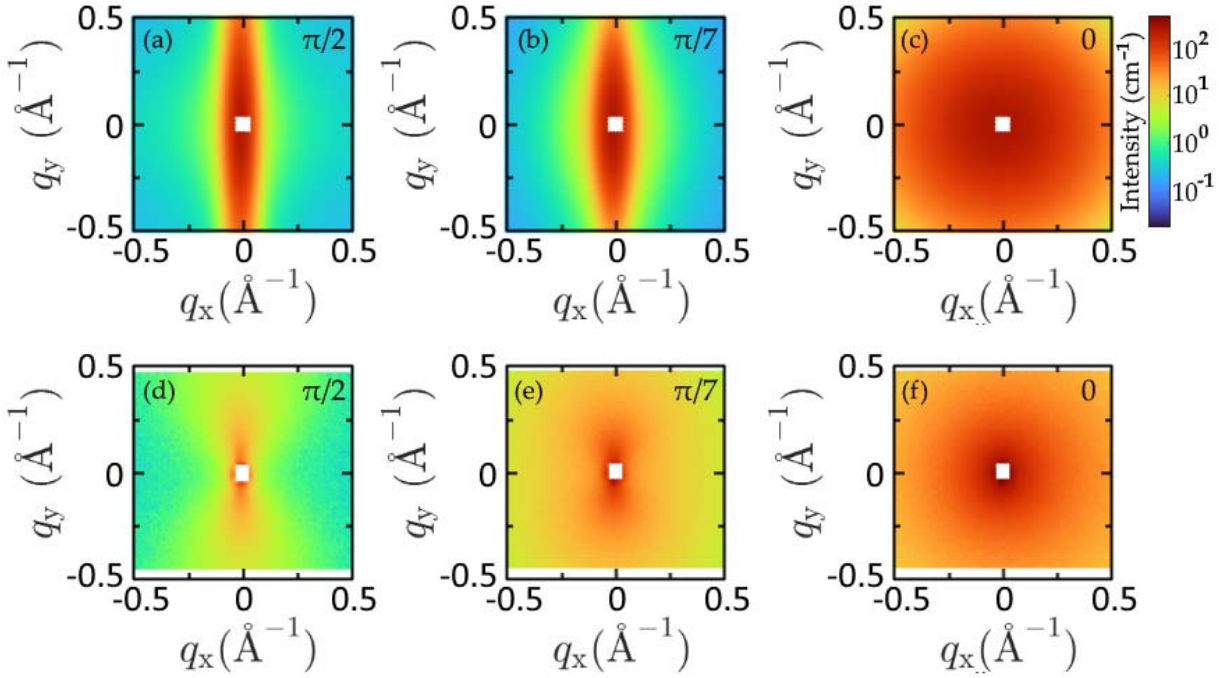

Fig. S1: Theoretical, (a) – (c), and experimental, (d) – (f), 2D small-angle scattering patterns generated from a theoretical suspension of rigid rods and from SANS measurements of a worm-like micelle solution, where the label in the upper right corner of each scattering image corresponds to θ_p.

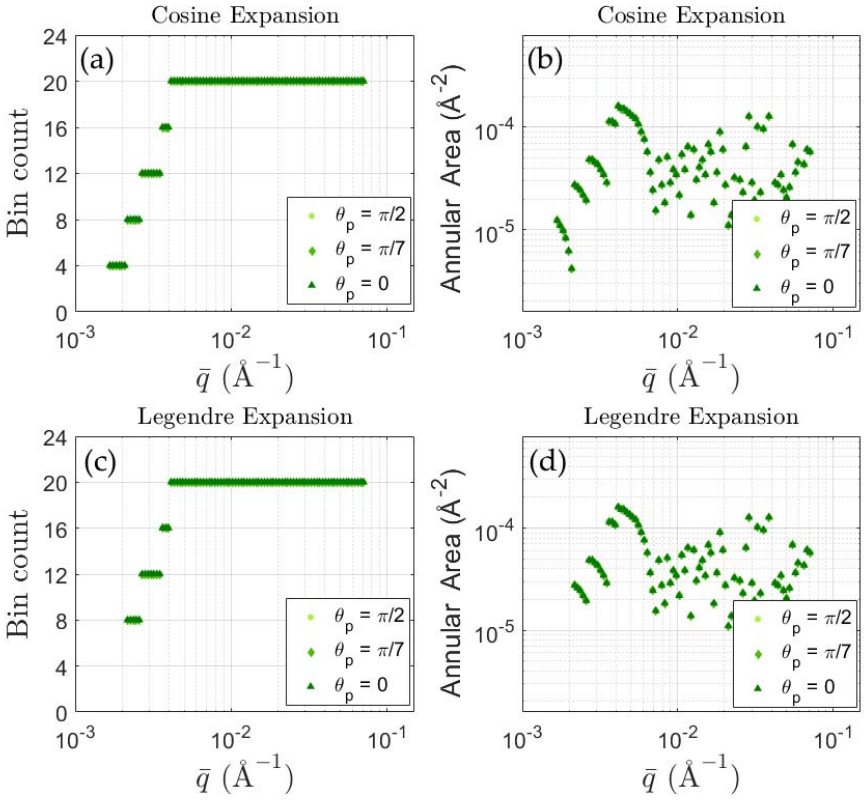

Fig. S2: The bin count (a, c) and annular area (b, d) used for cosine (a, b) and Legendre (c, d) expansion calculations of alignment factor for a smeared 2D theoretical scattering pattern of cylindrical particles having $L = 1800$ Å, $R = 20$ Å, and 5% radial polydispersity, where the alignment factor is reported in **Fig. 7**. The bin count and annular area is identical for each particle orientation, θ_p, such that points lie on top of each other.

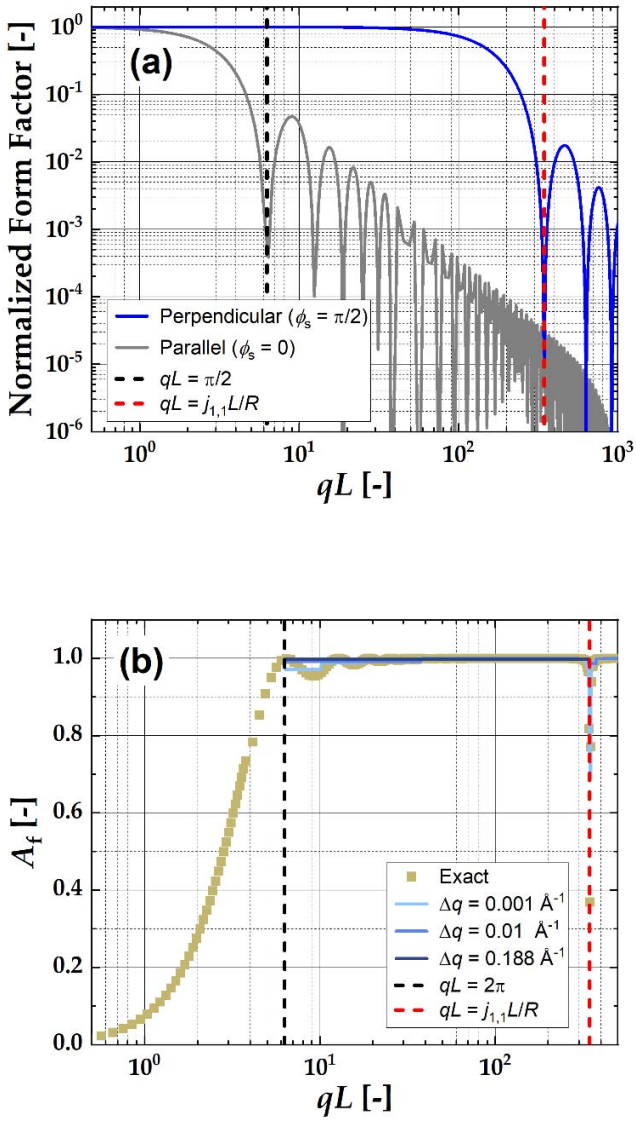

Fig. S3: (a) Scattering intensity curve of a theoretical cylinder with $L = 1800$ Å and $R = 20$ Å at $\theta_p = \frac{\pi}{2}$ along the $+q_y$ (perpendicular) and $+q_x$ (parallel) scattering axes *versus* dimensionless scattering vector, qL, illustrating the typical range of $2\pi \leq qL \leq j_{1,1}L/R$ for calculating (b) alignment factor, A_f, where the q-range, Δq, included in the integration changes A_f by < 3 %. The minimum of $qL = 2\pi$ corresponds to the peak of the first oscillation of the exact curve in (b), while the maximum at $qL = j_{1,1}L/R$ coincides with the first asymptote.

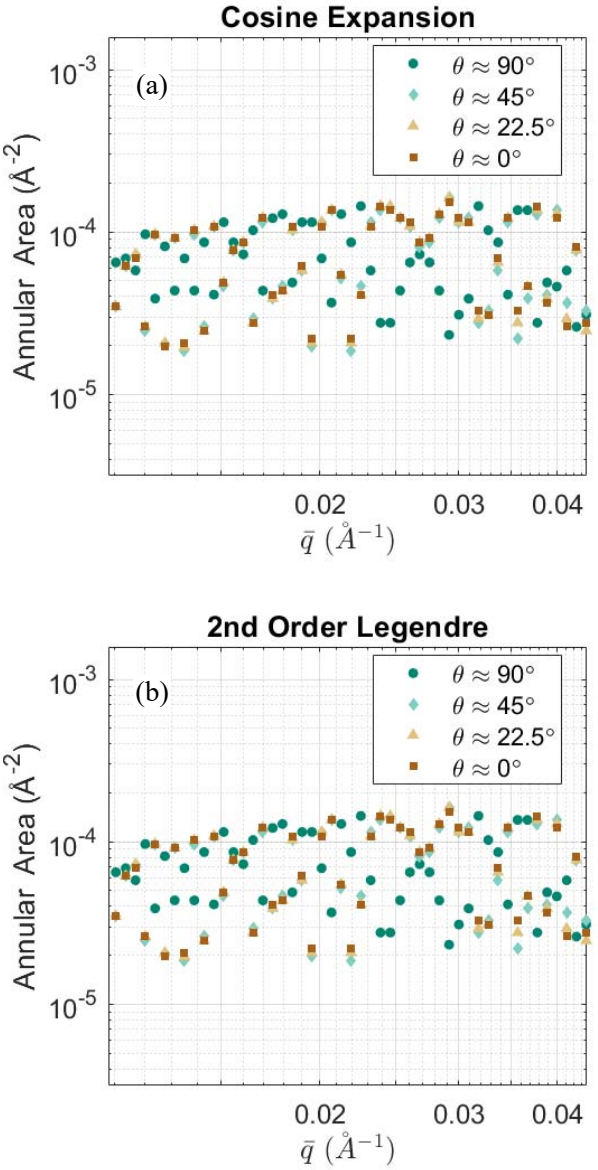

Fig. S4: Annular area, A_A, used to estimate alignment factor in **Fig. 9** for CTAB/NaSal WLM scattering data with the (a) cosine and (b) Legendre expansion methods, where annular area only depends on the requirement to have 20 evenly spaced bins containing at least one data point and is not correlated with average q-value, $\bar{q}$.